Strength of a Weak Bond Connecting Flexible Polymer Chains

Evan Evans*# and Ken Ritchie*

*Physics and Pathology, University of British Columbia, Vancouver, British Columbia V6T 1Z1, Canada, and #Biomedical Engineering, Boston University, Boston, Massachusetts 02215 USA

ABSTRACT Bond dissociation under steadily rising force occurs most frequently at a time governed by the rate of loading (Evans and Ritchie, 1997 *Biophys. J.* 72:1541–1555). Multiplied by the loading rate, the breakage time specifies the force for most frequent failure (called *bond strength*) that obeys the same dependence on loading rate. The spectrum of bond strength versus log(loading rate) provides an image of the energy landscape traversed in the course of unbonding. However, when a weak bond is connected to very compliant elements like long polymers, the load applied to the bond does not rise steadily under constant pulling speed. Because of nonsteady loading, the most frequent breakage force can differ significantly from that of a bond loaded at constant rate through stiff linkages. Using generic models for wormlike and freely jointed chains, we have analyzed the kinetic process of failure for a bond loaded by pulling the polymer linkages at constant speed. We find that when linked by either type of polymer chain, a bond is likely to fail at lower force under steady separation than through stiff linkages. Quite unexpectedly, a discontinuous jump can occur in bond strength at slow separation speed in the case of long polymer linkages. We demonstrate that the predictions of strength versus log(loading rate) can rationalize conflicting results obtained recently for unfolding Ig domains along muscle titin with different force techniques.

INTRODUCTION

Although many factors affect the cohesive strength of a material or the adhesive strength of attached interfaces, these properties are ultimately limited by the forces needed to break molecular bonds. In biology, the peculiar feature is that structures of most living organisms involve covalently bonded macromolecules interconnected by weak noncovalent interactions, which have finite lifetimes and thus will fail under any level of force if pulled on for a sufficient length of time. So when we speak of bond strength, we are thinking of the force that is most likely to break the bond on a particular time scale. Similarly, a well-defined peak in the distribution of single-bond detachment forces from probe tests reflects the limited period of survival of a bond under steadily rising load. Hence the force for most frequent failure (bond strength) is a dynamic property that depends on loading history as well as bond chemistry. Adding to complexity in soft material structures, bond breakage is driven by a nontrivial loading process that involves molecular compliance as well as rendering speed.

The objective here is to examine the effect of soft molecular linkages on the strength of a weak connecting bond under dynamic loading. The approach mimics typical laboratory experiments in which a weak bond linked to a probe and substrate by flexible polymers is broken through constant speed extension of the polymer chains. In the analysis, we have used generic mechanical models (Fixman and Kovac, 1973) to specify force-extension properties of the polymer linkages and Kramers' theory for reaction kinetics in liquids to model the frequency of bond dissociation under force (Evans and Ritchie, 1997). The polymer models include the wormlike chain (WLC), which best describes biopolymers like DNA or F-actin (Marko and Siggia, 1995), and the freely jointed chain (FJC), which describes linear homopolymers like polyethylene oxide. Compared to rupture of a bond linked rigidly to the probe and substrate, we will show that when connected by either polymer, the bond survives longer but fails at lower force under separation at the same speed. Moreover, long polymer linkages lead to major distortion of the spectrum of bond strength versus speed of separation and even to discontinuous jump-like transitions in strength at slow separation speeds. To demonstrate these important consequences, we will examine recent tests of force-driven unfolding of Ig domains in long chains of the muscle protein titin.

EXPERIMENTAL EXAMPLES

We begin by introducing the recent beautiful tests of titin extension by atomic force microscopy (AFM) (Reif et al., 1997) and laser optical tweezers (LOT) (Kellermayer et al., 1997; Tskhovrebova et al., 1997) to demonstrate rupture of bonds held by polymer linkages. Titin, a structural component of muscle, is a pearl chain of ~300 folded immunoglobulin (Ig) and related fibronectin type III (FN-III) domains connected by deformable proline-, glutamate-, valine-, and lysine-rich (PEVK) domains (Erickson, 1997). In the AFM test, Ig domains unbonded (unfolded) explosively as titin was extended by force, which contributed discrete jumps in length. As seen in Fig. 1 *a* (taken from Reif et al., 1997), the force rose nonlinearly with extension before each unbonding event and followed the form predicted for a WLC polymer. Not surprisingly, the unbonding event and jump in length occurred in the stiff asymptotic range of extension as the polymer was pulled taught. Thus the Ig domains experienced large forces for only a fraction of the loading time. From distributions obtained at many extension speeds, the most frequent forces for unfolding of Ig domains were found to increase as the logarithm of the separation speed in the AFM tests, as shown in Fig. 2. On the other hand, when anchored by an optical trap and pulled at comparable speeds, titin was observed to first extend elasti-

Received for publication 13 July 1998 and in final form 9 February 1999.

Address reprint requests to Dr. Evan A. Evans, Department of Physics, University of British Columbia, 6224 Agricultural Rd., Vancouver, BC V6T 1Z1, Canada. Tel.: 604-822-7579; Fax: 604-822-7635; E-mail: evans@physics.ubc.ca.

0006-3495/99/05/2439/09 $2.00

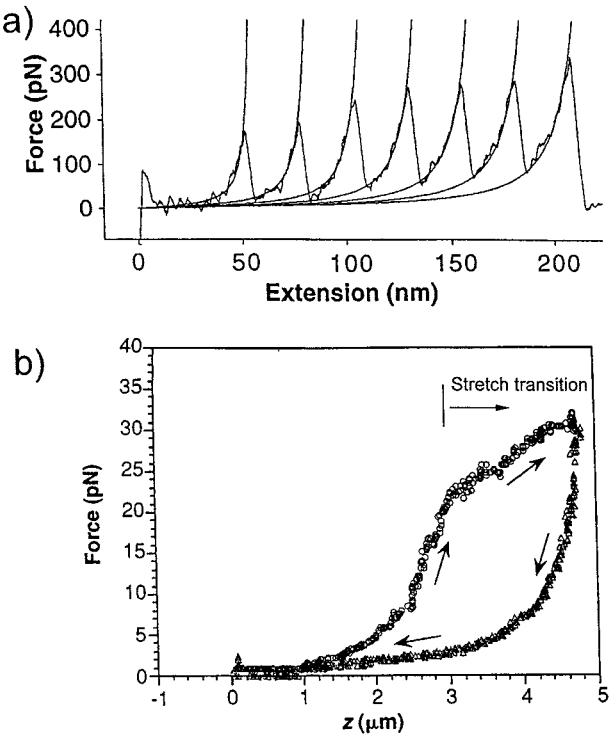

FIGURE 1 (*a*) Forces measured by AFM during extensions of recombinant constructs of eight immunoglobulin Ig domains of the muscle protein titin (taken from Reif et al., 1997). Folded into compact β-sheet structures, unfolding of each Ig domain shows up as a precipitous drop in force followed by a ~30-nm addition in length. As shown by the dotted line, force rises with extension of the added length, as predicted by the wormlike chain model and a persistence length of ~0.4 nm (Reif et al., 1997). (*b*) Forces measured by LOT during extension and release of a native titin strand (taken from Kellermayer et al., 1997). The initial stretch and final release phases follow the form predicted by the wormlike chain model, but with a much longer persistence length of ~2 nm. The abrupt change in slope during extension reflects a sequence of many (~70) unfolding events labeled as a "stretch transition" in Kellermayer et al., which accounts for the large hysteresis on release.

cally and then undergo a continuous inelastic "stretch transition" at much lower forces, as shown in Fig. 1 *b* (taken from Kellermayer et al., 1997). The elastic regime of titin elongation again followed the form predicted for a WLC polymer, and the inelastic extension was also attributed to unfolding of Ig domains. However, the forces for onset of unfolding Ig domains in the LOT tests seemed to deviate significantly from the AFM values, as seen in Fig. 2. Based on theory, we will show that the apparent discrepancy between AFM and LOT tests vanishes for the most part when we recognize the difference between force constants in the two techniques. Moreover, we will show that nonsteady loading played an important role in the process of unbonding in both experiments and that we must account for compliance of the long titin chain to extract reliable properties of the unfolding kinetics for Ig domains. (Although it is a similar type of LOT test, we do not show results from Tskhovrebova et al. (1997) because the principal emphasis of their paper was on force relaxation versus time after steps of ~250-nm extension of titin. In contrast to force relaxation at static extension, our interest here is to examine dissociation of a weak bond connected by polymer chains under constant speed extension.)

THEORY OF BOND BREAKAGE IN LIQUIDS

As background, we first give a brief review of the stochastic process of bond dissociation under a ramp of force (Evans and Ritchie, 1997). Then we enlarge the analysis to show how soft-polymer linkages affect loading and alter the expected breakage force. In modeling the kinetics of dissociation, we take advantage of the enormous gap in time scale that separates thermal-Brownian impulses in liquids ($\sim 10^{-12}$ s or shorter) from force changes in laboratory probe experiments ($\sim 10^{-4}$ s or longer). Hence the ultrafast dynamics are analyzed under the assumption of constant applied force using the statistical mechanics theory of Kramers (Kramers, 1940; Hanggi et al., 1990). This step yields a kinetic rate or frequency $\nu(f)$ for bond dissociation that depends on the level of force. Next, bond breakage in a laboratory test is treated as a first-order Markov process with increasing rate of dissociation driven by the rising force. The outcome is a distribution of breakage forces whose breadth and peak location (bond strength) depend on the rate at which force is applied to the bond.

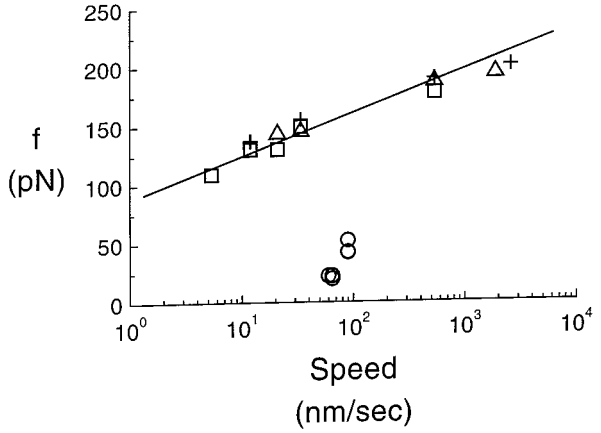

FIGURE 2 Plot of force versus log(pulling speed) for unfolding Ig domains under titin extension. Results from the AFM stretch of ~500 nm pieces of native titin are grouped along the straight line (taken from Reif et al., 1997). Well below the AFM data, open circles are forces for the onset of unfolding at stretch transitions in the LOT tests of micron-length titin (taken from Kellermayer et al., 1997).

Rate of dissociation under force

Although energy landscapes governing strengths of bonds can be complex, with many pathways for unbonding, we idealize a bond as confinement by a single energy barrier positioned along a specific reaction path, which is selected by the external pulling force. Starting far from equilibrium with all states inside the barrier, the kinetics of dissociation in Kramers' theory are treated as a stationary flux of probability density along this preferential path from the deep energy minimum outward past the barrier via a saddle point in the energy surface. For overdamped liquid environments, this transport is modeled by the Smoluchowski equation. Mapped on a scalar coordinate x, the energy landscape $E(x)$ is assumed to be bounded by steeply rising energy in other directions. With some orientation θ relative to the molecular coordinate, application of external force to the bond adds a

mechanical potential $-fx\cos(\theta)$ that tilts the energy landscape and diminishes the energy barrier E_b at the transition state. When the deformed energy landscape is introduced into Kramers-Smoluchowski theory, a generic expression is found for the frequency of dissociation, which depends on applied force (Evans and Ritchie, 1997):

$$\nu \approx (D/l_c l_{ts}) \exp[-E_b(f)/k_B T]$$

where the energy scale is set by thermal energy $k_B T$. The diffusive nature of overdamped kinetics is embodied in an attempt frequency $D/l_c l_{ts}$, or inverse diffusion time $t_D = l_c l_{ts}(\gamma/k_B T)$, governed by viscous damping γ and two length scales. The first length l_c is the thermal spread in the bound state, which defines the gradient in the density of states ($\sim 1/l_c$) that drives dissociation. In a harmonic approximation, l_c is derived from curvature $\kappa_c = (\partial^2 E/\partial x^2)_c$ of the energy landscape local to the minimum, i.e., $l_c = (2\pi k_B T/\kappa_c)^{1/2}$. The second length l_{ts} is the energy-weighted width of the barrier $l_{ts} = \int dx \cdot \exp[\Delta E(x)_{ts}/k_B T]$ at the transition state at $x = x_{ts}$, which is also derived from curvature $\kappa_{ts} = (\partial^2 E/x^2)_{ts}$ of the energy landscape, i.e., $l_{ts} = (2\pi k_B T/\kappa_{ts})^{1/2}$. For physical potentials that vary with distance, force can displace and change the barrier width [i.e., $1/l_{ts} = (\kappa_{ts}/2\pi k_B T)^{1/2} \approx g(f)$], which contributes a weak force-dependent prefactor $g(f)$ to the rate expression. [For simple physical potentials, the prefactor $g(f)$ is $\sim f^a$; values of the exponent range from $a \approx 1/2$ for inverse power law attractions to $a \approx 1$ for capture in a deep harmonic well (Evans and Ritchie, 1997).] Even so, the major impact of force on the frequency of dissociation comes from changes in the thermal likelihood of reaching the top of the energy barrier, $\exp[-E_b(f)/k_B T]$. For highly curved barriers, the location of the transition state x_{ts} remains approximately constant under force, so the barrier is lowered in proportion to a fixed distance x_β, i.e., $E_b(f) \approx E_b - f \cdot x_\beta$, which is the thermally averaged projection $x_\beta = \langle x_{ts}\cos(\theta)\rangle$ of the transition state along the direction of force. Thus, reflecting thermal activation, the characteristic force scale is given by the ratio of thermal energy to the distance x_β, i.e., $f_\beta = k_B T/x_\beta$, which can be surprisingly small, because $k_B T \approx 4.1$ pN · nm at room temperature and $x_\beta \approx 0.1$–1 nm. As force rises on this scale, the analysis of dissociation past a single barrier predicts the following expression for the kinetic rate:

$$\nu \approx (1/t_o)\, g(f/f_\beta) \exp(f/f_\beta) \tag{1}$$

which is dominated by an exponential in force, as first postulated by Bell (1978). Kramers' classic result for thermally activated kinetics sets the frequency scale, $1/t_o = (1/t_D)\exp(-E_b/k_B T)$.

Driven stochastic process of bond breakage in probe tests

As illustrated earlier (cf. Fig. 1), surfaces in laboratory tests of bond strength are usually separated at constant speed after contact. Therefore, the load applied to a bond is not fixed. If the bond is attached rigidly to the probe tip and substrate, the load increases at a constant rate $\Delta f/\Delta t = k_f v_t$ as determined by the speed v_t of separation and stiffness k_f of the transducer. For rupture forces on the order of 100 pN, the force ramp spans time periods greater than 10^{-4} s before bond rupture, even with the fast AFM ($\Delta f/\Delta t \approx 10^4$ to 10^6 pN/s). The mechanical loading is extremely slow compared to thermal impulses lasting more than 10^{-12} s, so the assumption of stationary force in the statistical mechanics of dissociation is valid. However, because the force increases with time, the frequency of bond failure increases under probe separation. Moreover, as force rises above the thermal force scale, molecular states beyond the energy barrier are convected apart by force faster than can be recombined by diffusion. Hence, the rate of reassociation (on rate) is overwhelmed by force, and bond breakage reduces to a first-order Markov process with a time-dependent off rate, i.e., $\nu[f(t)]$. The likelihood of bond survival up to time t is found by integration of the rate of dissociation, i.e., $\exp\{-\int_o^t \nu[f(t')] \cdot dt'\}$, which is then multiplied by the dissociation rate to obtain the probability density of failure within a small interval of time $[t, t + dt]$:

$$p(t) = \nu[f(t)] \cdot \exp\left\{ -\int_{o\to t} \nu[f(t')] \cdot dt' \right\}$$

For constant speed separation and perfectly elastic linkages to the bond, the force experienced by the bond is a deterministic function of time. Thus the probability of failure $p(f) \cdot df$ in a small increment of force is equivalent to the probability within the small interval of time $p(t) \cdot dt$ as related by the loading-time transformation, $dt = (1/v_t)(\partial x/\partial f)df$, i.e.,

$$p(f) = \nu(f) \cdot [(1/v_t)(\partial x/\partial f)] \cdot \exp\left\{ -\int_{o\to f} \nu(f') \cdot [(1/v_t)(\partial x/\partial f)] \cdot df' \right\} \tag{2}$$

where $(\partial x/\partial f) = 1/k_f + (\partial x_p/\partial f)$ is the total elastic compliance (extension/force) defined by transducer $1/k_f$ and polymer $\partial x_p/\partial f$ compliances. Introducing the generic form for off rate from Eq. 1, the probability density becomes a function of dimensionless force $f \equiv f/f_\beta$ and time $\tau \equiv t/\tau_f$,

$$p(f) = (\tau_f/t_o) \cdot (\partial\tau/\partial f) \cdot g(f) \cdot \exp\left\{ f - (\tau_f/t_o) \int_{o\to f} (\partial\tau/\partial y) \cdot g(y) \cdot \exp(y) \cdot dy \right\} \tag{3}$$

where $\tau_f = f_\beta/(k_f v_t)$ is the apparent time needed for the probe force to reach the thermal force f_β. In this dimensionless form, the loading time function $(\partial\tau/\partial f)$ reduces to the dimensionless total compliance $c(f) = [1 + k_f(\partial x_p/\partial f)]$. This leaves the distribution of breakage forces in Eq. 3

parameterized by a dimensionless rate of loading $r_f = (t_o/\tau_f) = k_f v_t/(f_\beta/t_o)$. The loading rate scale defined by f_β/t_o represents the thermal activation threshold beyond which bonds are driven from equilibrium and exhibit strength. If n identical bonds are linked in series, the loading history remains the same, but the frequency of dissociation is increased by a factor n, which rescales the dimensionless loading rate $r_f = k_f v_t/(nf_\beta/t_o)$. With compliant linkages, the dimensionless loading rate defined by r_f is only an apparent loading rate (equivalent to separation speed) because the bond experiences a nonuniform buildup of force.

Most important, the probability density for bond breakage is the product of an off rate that increases with time multiplied by the likelihood of bond survival that decreases with time. Thus a maximum can occur in the distribution at a specific time. The peak defines the most likely force f^* for bond breakage, which is commonly identified as bond strength. Analytically, the most likely breakage force is derived from a maximum in the distribution, i.e., $\partial p/\partial f = 0$. The result is a transcendental equation that relates the location of the dimensionless strength f^* to the dimensionless loading rate r_f,

$$f^* = \ln(r_f) + \ln\{[\partial \ln(c)/\partial f + \partial \ln(g)/\partial f + 1]/c(f)\cdot g(f)\}_{f=f^*} \quad (4)$$

In the case of a very sharp energy barrier where we can neglect the force-dependent prefactor $g(f)$ in the dissociation rate, Eq. 4 predicts that bond strength increases in direct proportion to $\log_e$(loading rate) for a rigidly connected bond [i.e., $c(f) \equiv 1$]. On the other hand, because the compliance function $c(f)$ and its derivative $\partial \ln(c)/\partial f$ appear in Eq. 4, we see that bond strength can be shifted in nontrivial ways when linked to nonlinear elastic components like polymers.

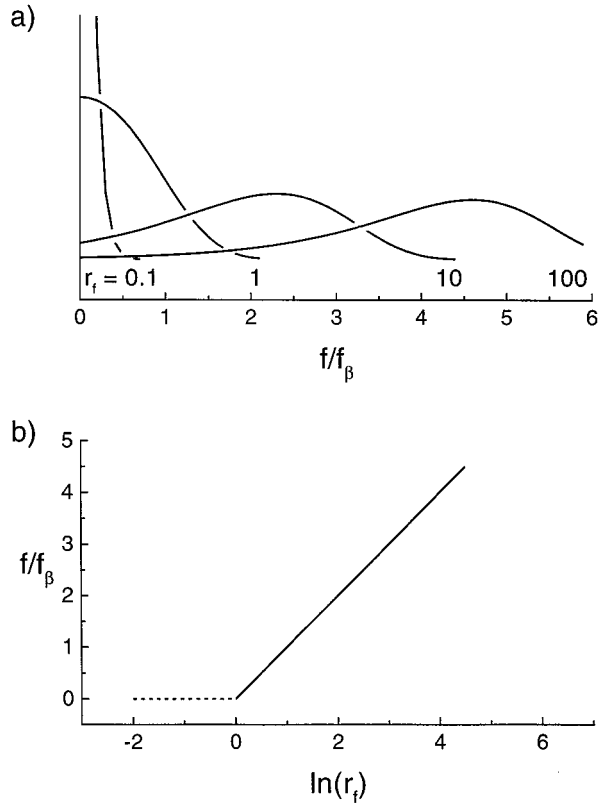

FIGURE 3 (*a*) Probability densities (vertical axis, arbitrary scale) calculated over a three-order-of-magnitude range in loading rate for breakage of a bond linked rigidly to the origin of force. Idealized as a sharp activation barrier at fixed location, the kinetic rate for thermally activated dissociation is predicted to increase with force as $\nu \approx (1/t_o)\exp(f/f_\beta)$. Force f and loading rate r_f scales are set by thermal activation parameters $f_\beta = k_B T/x_\beta$ and $f_\beta/t_o = (f_\beta/t_D)\exp[-E_b/k_B T]$, respectively. (*b*) The spectrum of most frequent breakage force (strength) versus logarithm of loading rate is a straight line.

Weak bonds held by rigid linkages

We now establish comparative baselines for strength based on a rigidly linked bond [$c(f) \equiv 1$] and two models of the bonding potential. The first model is a sharp barrier at a fixed location x_β along the unbonding pathway where the off rate is given by $\nu \approx (1/t_o)\exp(f/f_\beta)$. The second model is a deep harmonic well where the off rate is approximated by $\nu \approx (1/t_o)(f/f_\beta)\exp(f/f_\beta)$. Calculated from Eqs. 3 and 4, normalized distributions of breakage forces and spectra of strength versus $\log_e$(loading rate) are plotted in Figs. 3 and 4, respectively, for each model. As discussed in detail elsewhere (Evans and Ritchie, 1997), some distinct features and dynamic regimes are immediately evident. First, strength emerges at a threshold loading rate. Below the threshold rate, spontaneous dissociation dominates the statistics of failure, and the peak in a distribution of breakage forces stays at zero force. For a sharp barrier, the dimensionless threshold rate is identically 1 ($r_f^* = 1$), whereas for physical potentials like the harmonic well, the dimensionless threshold rate is <1. On the other hand, both models cross over to an essentially universal regime once $r_f > 1$, where strength rises in proportion to the logarithm of the loading rate [$f^* \approx f_\beta \ln(r_f)$]. The linear proportionality reflects e-fold reductions in activation energy with force increments of f_β. Labeled as the fast loading regime, the logarithmic increase spans many decades of loading rate determined by the barrier energy E_b. However, in complex bonds, a cascade of sharp activation barriers can be traversed along the force-driven unbinding pathway. In this case, there will be a sequence of linear regimes with ascending slopes set by the locations of each barrier, as demonstrated in recent experiments with receptor-ligand bonds (Merkel et al., 1999). Ultimately, although not shown here, the spectrum of strength versus log(loading rate) reaches an ultrafast regime when the dimensionless rate $r_f > \sim\exp(E_b/k_B T)$. In this regime, forces quickly exceed the bare strength f_∞ set by the maximum gradient of the bonding potential and overwhelm the energy barrier. These loading rates are extremely fast ($\sim 10^{12}$ pN/s) and are only realized in molecular dynamics (MD) simulations.

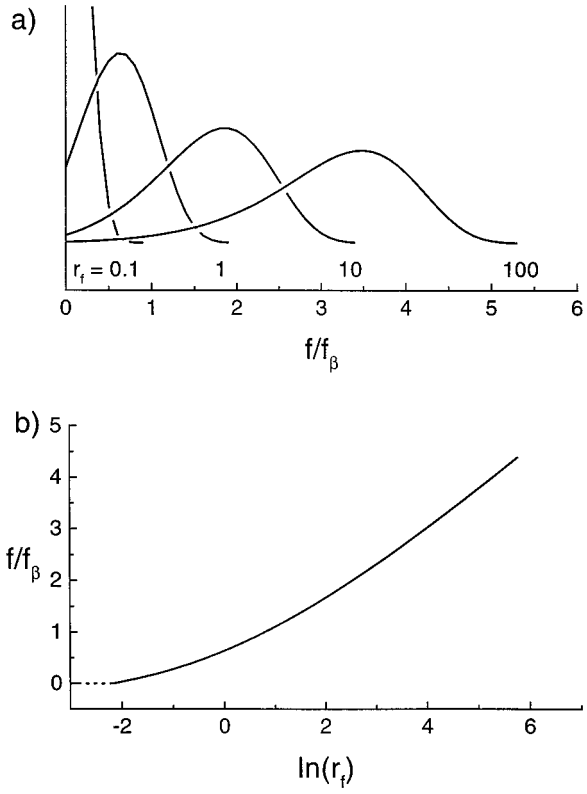

FIGURE 4 (*a*) Probability densities (vertical axis, arbitrary scale) calculated over a three-order-of-magnitude range in loading rate for breakage of a bond linked rigidly to the origin of force. Idealized as a deep harmonic well potential, the kinetic coefficient for thermally activated dissociation is predicted to increase with force as $\nu \approx (1/t_o)(f/f_\beta)\exp(f/f_\beta)$. Force f and loading rate r_f scales are set by thermal activation parameters $f_\beta = k_BT/x_\beta$ and $f_\beta/t_o = (f_\beta/t_D)\exp[-E_b/k_BT]$, respectively. (*b*) The spectrum of most frequent breakage force (strength) versus logarithm of loading rate approaches a straight line for $f > 1$.

Weak bonds held by polymer chains

For soft linkages, the bond is subjected to low force for long periods and can fail at lower force than would be expected from the apparent loading rate of the probe. To see this, consider the trivial model where the linkages behave as weak elastic springs represented by the constant k_L (force/extension). In this case, the compliance function is the well-known relation $c(f) = (k_L + k_f)/k_L$ for linear springs in series. For constant compliance, the force distributions and strength peaks shown in Figs. 3 and 4 remain unchanged, except that all are shifted to the right on the $\log_e$(apparent loading rate) scale by $\log_e[(k_L + k_f)/k_L]$. Hence, at any value of apparent loading rate, the bond strength is lowered by $-f_\beta\log_e[(k_L + k_f)/k_L]$, and a higher apparent rate of loading is needed to reach the threshold for the onset of bond strength. In the case of nonlinear elastic components like polymers, the analysis is not as simple because the rate of force increase under steady separation is not constant. Response to constant speed extension involves viscous and elastic forces along the polymer chain (Doi and Edwards, 1986). At extreme pulling speeds, thermal randomization of polymer configurations will be slower than the smoothing action of the mechanical extension. At high speeds, force is dominated by viscous drag and propagates along the chain (Seifert et al., 1996). On the other hand, at slow pulling speeds, the chain will be sufficiently randomized so that the local average force along the chain is close to the equilibrium elastic limit. In the analysis to follow, we restrict our treatment to the quasielastic regime of slow pulling speeds. In the Appendix, we estimate bounds on pulling speed that limit the quasielastic regime for each type of polymer. In the experiments described earlier, the speed of titin extension was well below the bound estimated for a WLC polymer.

Assuming quasiequilibrium at all extensions x_p ($= x_p/L_p$), force arises from reduction in configurational entropy of the polymer. The force-length relation depends only on the fully stretched length L_p of the polymer, the statistical segment or persistence length b, and temperature (Fixman and Kovac, 1973). In the model of a freely jointed chain, force begins as $f \approx 3(k_BT/b)x_p$ at small extensions $x_p \ll 1$ but ultimately stiffens to increase as $f \to k_BT/[b(1 - x_p)]$ near limiting extensions $x_p \to 1$. In the stiffer wormlike chain, force begins as $f \approx 3(k_BT/b)x_p/2$ and finally increases as $f \to k_BT/[4b(1 - x_p)^2]$ when $x_p \to 1$. Following the approach used by Marko and Siggia (1995), we have used simple interpolations to approximate the force over the full range of polymer extension. The relations match both the linear harmonic regime at small extension and the stiff asymptotic regime at large extension:

$$\text{FJC:}\quad f \approx (k_BT/b)[x_p(3 - 2x_p)/(1 - x_p)]$$

$$\text{WLC:}\quad f \approx (k_BT/b)[x_p(6 - 9x_p + 4x_p^2)/4(1 - x_p)^2]$$

The overall compliance of these linkages in series with the transducer is derived from the increase in total separation x ($= x_t + x_p$) with force as given by $\partial x/\partial f = 1/k_f + \partial x_p/\partial f$. When multiplied by transducer stiffness k_f and scaled by thermal force f_β, the compliance function $c(f)$ is left parameterized by the characteristic ratio of transducer:polymer stiffnesses $c_p = k_fL_pb/(k_BT)$ and the ratio of molecular lengths x_β/b, which we take as order unity (i.e., $x_\beta/b \approx 1$). Hence, the following relations were used to specify the compliance functions for the two polymer models:

$$\text{FJC:}\quad c(f) \approx \{1 + c_p(1 - x_p)^2/[1 + 2(1 - x_p)^2]\}$$

$$\text{WLC:}\quad c(f) \approx \{1 + 2c_p(1 - x_p)^3/[1 + 2(1 - x_p)^3]\}$$

which are implicit functions of force through $x_p(f)$. Starting from $c_p = 0$ for rigid linkages, the compliance parameter c_p in experiments can range upward to values greater than 10^4 for long polymers ($L_p \approx 100$ nm) and stiff AFM cantilevers ($k_f \approx$ N/m)!

Using the two chain models and the two idealizations of bonding, we have calculated distributions of breakage forces and spectra of strength versus $\log_e$(apparent loading rate) defined by the product of separation speed and transducer stiffness. As shown in Figs. 5 and 6, the expected level of bond strength at a given separation speed depends

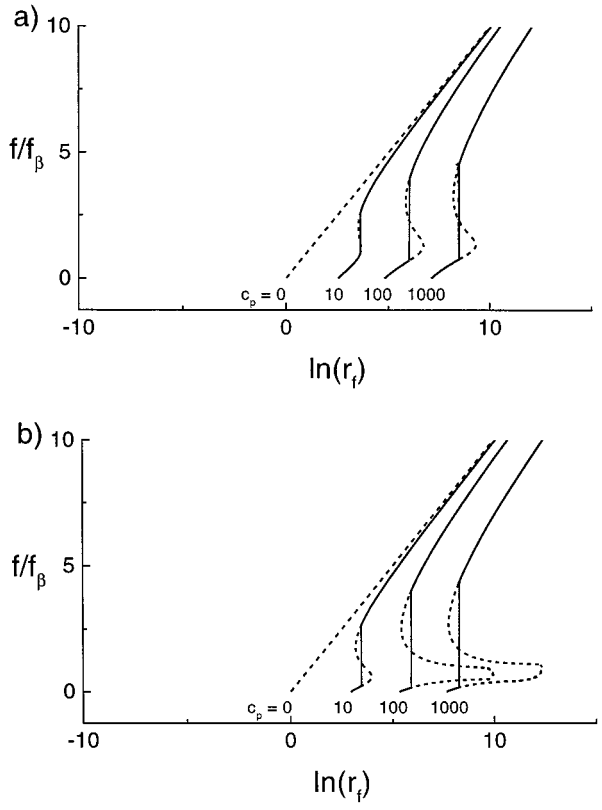

FIGURE 5 Spectra of bond strength versus logarithm of apparent loading rate (transducer stiffness × separation speed) for breakage of a bond idealized as a sharp activation barrier at fixed location. The dashed straight lines are the prediction of strength versus log(loading rate) taken from Fig. 3 *b* for a rigid linkage. (*a*) The probe is assumed to be linked to the bond by freely jointed polymer chains. (*b*) The probe is assumed to be linked to the bond by wormlike polymer chains. The compliance parameter c_p defines the ratio of the transducer stiffness to the characteristic stiffness of each polymer, i.e., $c_p = k_f L_p b/(k_B T)$. The solid curves show that soft linkage of a bond to a stiff probe or substrate can lead to significant reduction in strength—even an abrupt transition—at low apparent loading rates. Force f and apparent loading rate r_f scales are set by thermal activation parameters $f_\beta = k_B T/x_\beta$ and $f_\beta/t_o = (f_\beta/t_D)\exp[-E_b/k_B T]$, respectively.

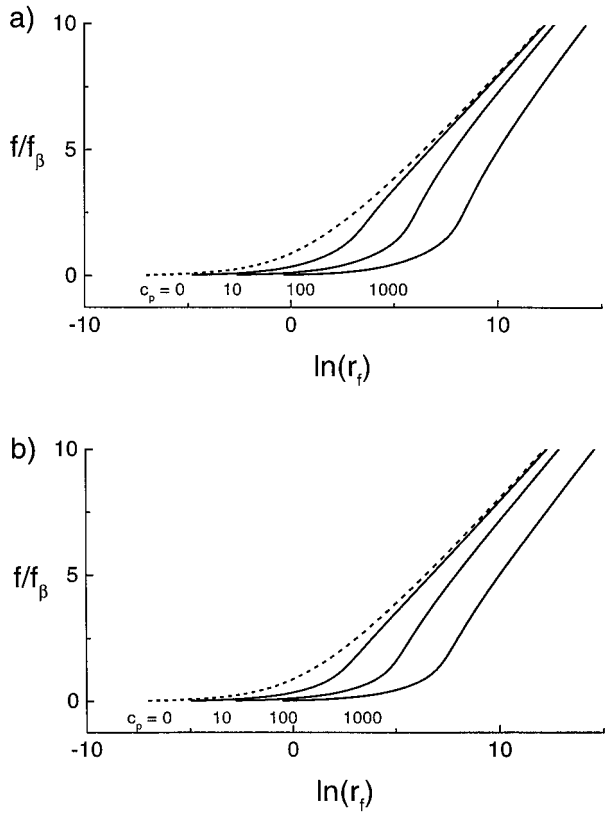

FIGURE 6 Spectra of bond strength versus logarithm of apparent loading rate (transducer stiffness × retraction speed) for breakage of a bond idealized as a deep harmonic well. The dashed curves are the prediction taken from Fig. 4 *b* for a rigid linkage. (*a*) The probe is assumed to be linked to the bond by freely jointed polymer chains. (*b*) The probe is assumed to be linked to the bond by wormlike polymer chains. The compliance parameter c_p defines the ratio of the transducer stiffness to the characteristic stiffness of each polymer, i.e., $c_p = k_f L_p b/(k_B T)$. The solid curves show that soft linkage of a bond to a stiff probe or substrate can lead to significant reduction in strength (but without abrupt transition) at low apparent loading rates. Force f and apparent loading rate r_f scales are set by thermal activation parameters $f_\beta = k_B T/x_\beta$ and $f_\beta/t_o = (f_\beta/t_D)\exp[-E_b/k_B T]$, respectively.

on the ratio c_p of transducer stiffness to the characteristic stiffness of the polymer linkage. It is clearly evident that the effect of a soft polymer linkage is most prominent at low speeds. The reason for the major reduction in strength at low pulling speed is that the bond has a lot of time to break at low force before the polymer chain is pulled taught. Once taught, the force transmitted by a chain rises at the loading rate set by the transducer stiffness and separation speed. Likewise, because of the protracted period at low force, the threshold rate of loading where strength is first perceived moves to higher speeds in approximate proportion to the compliance parameter c_p, i.e., $r_f^* \approx (1 + 2c_p/3)$. What is more subtle in Figs. 5 and 6 is that a first-order dynamical transition can occur at low separation speeds in the case of a sharp energy barrier but not in the case of the deep harmonic well. The discontinuous jump in bond strength at a particular separation speed reflects the coexistence of two peaks in the distribution of breakage forces, as illustrated in Fig. 7 *a*. For the harmonic well, a single peak persists, but the distribution broadens then narrows again over the low speed range, as seen in Fig. 7 *b*. A second peak in the probability density of unbonding events is the obvious signature of a first-order type of transition. The simple way to conceptualize the split in distribution of unbonding events is to view the polymer/transducer linkage as a spring with two spring constants: a low value $k_p \approx k_B T/bL_p$ for extensions $x < L_p$ set by the polymer harmonic limit and a high value k_f when $x \geq L_p$, given by the transducer stiffness. Each of these spring states implies a distribution of unbonding events peaked at force values set by the logarithm of two loading rates, i.e., $f \approx f_\beta \ln(k_p v_t)$ and $f \approx f_\beta \ln(k_f v_t)$. So if pulled slowly, there will be a crossover where failure events will essentially be split between unbonding under low loading rates and high loading rates.

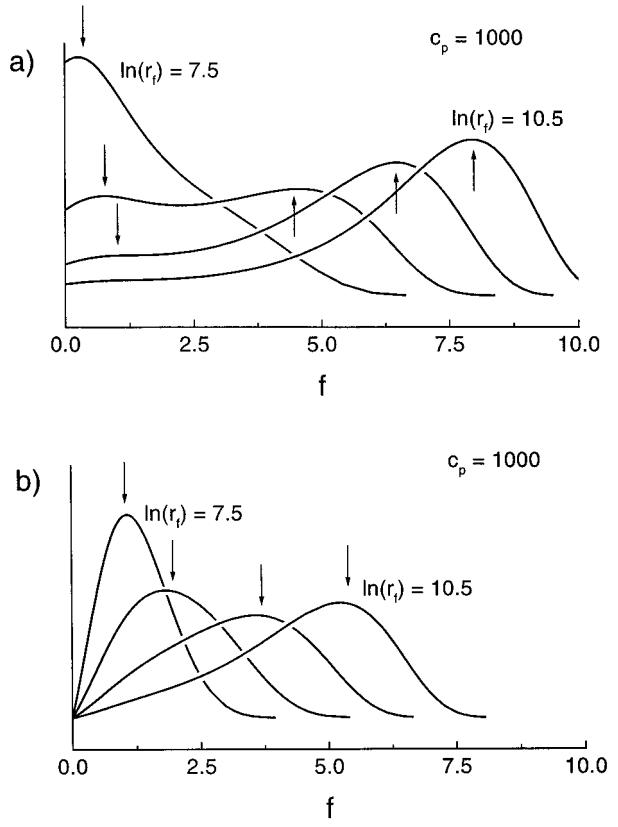

FIGURE 7 Probability densities (vertical axis, arbitrary scale) for breakage of a bond calculated over the low range of apparent loading rate (transducer stiffness × retraction speed). The bond is assumed to be linked to the probe and substrate by freely jointed chains. The ratio of the transducer stiffness to the characteristic stiffness of the polymer chains (c_p = 1000) was chosen to represent long polymers and a stiff transducer. (*a*) For a bond idealized as a sharp activation barrier at fixed location, two peaks appear in breakage force distributions at low rates of separation, which accounts for the discontinuous transition in bond strength. (*b*) For a bond idealized as a deep harmonic well, a single peak remains in breakage force distributions and shifts continuously to higher forces as the rate of separation is increased. Force f and apparent loading rate r_f scales are set by thermal activation parameters $f_\beta = k_BT/x_\beta$ and $f_\beta/t_o = (f_\beta/t_D)\exp[-E_b/k_BT]$, respectively.

UNFOLDING OF Ig DOMAINS IN TITIN EXPERIMENTS

In the two titin stretch experiments described earlier, different levels of force were needed to unfold Ig domains at comparable extension speeds (cf. Fig. 2). As shown by our analysis of bond dissociation under force, the measurements should be compared on a scale of the apparent loading rate defined by the product of transducer stiffness and separation speed (i.e., $k_f v_t$). Quite importantly here, the AFM transducer stiffness (~60 pN/nm) was more than 100-fold larger than the stiffness (~0.2 pN/nm) of the LOT particle trap. Multiplying the speed of extension by the appropriate stiffness accounts for the much lower forces observed in the LOT experiments, but the unfolding forces still approach zero with diminishing speed faster than the AFM results. We will see that this drop is consistent with the theoretical prediction shown in Fig. 5 *b* for a WLC polymer linkage with the exceptional compliance of titin. To correlate the prediction of force versus log(apparent loading rate) with the two sets of experimental data, we need to know the compliance parameter $c_p = k_f L_p b/(k_BT)$ and number n of Ig domains available for unfolding along titin in each case. For the force data taken from the reports, the stretched lengths of titin were longer (~2–5 μm) in the LOT tests than in the AFM tests (~500–800 nm); also, the persistence lengths used to model the WLC elasticity were longer (~2 nm for the LOT tests and ~0.4 nm for the AFM tests). (The value of persistence length needed to correlate the elastic response of titin is very important but is unresolved at present. According to Kellermayer et al. (1997), the value for a single strand of titin is 1.8 nm, and smaller values reflect multiple strands. As such, the value of ~0.4 nm in the AFM tests would indicate at least three strands, and thus normalized per strand, the force would be reduced significantly. On the other hand, Tskhovrebova et al. (1997) state that two pairs of contour and persistence lengths (representing low- and high-force behavior) are needed to characterize the elasticity of titin due to the differential character of the PEVK domain.) With these parameters, the dimensionless ratios of transducer stiffness to polymer stiffness differ by an order of magnitude or less, i.e., $c_p \approx 3000$ for the AFM experiment and $c_p \approx 400$ for the LOT experiment, which are much closer in value than expected from the large difference in transducer stiffnesses. Although native titin has ~300 Ig and FN-III domains (Erickson, 1997), there were differences in the number of sites available for unfolding between the two experiments, because different lengths of titin were subjected to stretch. For example, ~100 domains were unfolded in the longest extensions of titin by LOT, but only a few were unfolded in each AFM test.

To model unfolding force versus log(apparent loading rate), we assume that the energy landscape traversed in unfolding an Ig domain is dominated by a sharp barrier and that forces are transmitted through a WLC linkage. As such, the force-driven kinetics of unfolding are represented by $\nu \approx (1/t_o)\exp(f/f_\beta)$. If only one Ig domain existed in the titin chain, we would simply choose the dimensionless curve in Fig. 5 *b* for the appropriate value of c_p, then find the thermal force f_β (equivalent to a barrier location x_β) and off rate prefactor $1/t_o$ to match the experimental scale set by unfolding force and apparent loading rate. However, there are many sites for unfolding. Assuming that the n sites are identical, the spectrum of unfolding force remains the same and the prefactor $1/t_o$ is simply replaced by n/t_o to reflect the multiple kinetic processes occurring along the chain. To analyze a sequence of unfolding events, we must specify the intervening loading process. In the AFM tests, the force dropped significantly after each unfolding step before rising again with a similar WLC response. Thus each successive event in the AFM test was a new test with one less site for unfolding and a slightly longer contour length. (A subtle point is that the unfolding of Ig domains increased the

flexible length of the chain and thus altered the elastic response. Such progressive softening of the chain means that each experimental event should be characterized by a specific ratio of transducer:polymer stiffness c_p, which would require a cross map between the different force versus log(apparent loading rate) curves at fixed ratio. However, the dependence on this ratio is logarithmic, so the effect is weak and, interestingly, would be offset to some extent by the logarithmic shift due to the reduction in number of sites for unfolding (which scales the frequency or rate of unfolding).) Because only a few sites were unfolded in the stretch of native titin, no $\Delta\log(n)$ broadening is apparent in the results; but a reduction in the number of sites could account for the noticeable increase in force as Ig domains were unfolded in examples of short recombinant titin segments (Reif et al., 1997). On the other hand, for the LOT tests, the onset of a "stretch transition" is an initial unfolding event in a series of tens to hundreds of subsequent unfolding events. Because all of the sites experienced the same force history until the initial unfolding event, theory predicts that the most likely force for a second unfolding event should increase by $\sim f_\beta/n$ as $n \rightarrow n - 1$. The steady hysteretic extension in a stretch transition implies that successive unfolding events occurred at a nearly constant rate, i.e., $\sim v_t/L_{Ig}$, where the length increment per event under large force should have been close to $L_{Ig} \approx 30$ nm. Neglecting fluctuations in loading due to the length insertions, we expect that the most frequent unfolding force should rise at an approximate rate of $(f_\beta/n)v_t/L_{Ig}$. In the LOT tests, the rate of force increase after onset of the stretch transition was ~0.3 pN/s for steady elongation at speeds of ~65 nm/s.

Because of uncertainties in persistence length (titin test length) and number of unfolding sites, we will simply choose $c_p \approx 10^3$ *and* $n \approx 10^2$ to represent both titin experiments. Focusing on discrete unfolding events, we have correlated the dimensionless prediction of bond strength versus log(apparent loading rate) from Fig. 5 *b* with experimental data of unfolding force versus log(transducer stiffness × pulling speed). Shown in Fig. 8, the prediction was matched to the experimental scale by selecting the thermal force $f_\beta = 12.5$ pN (a barrier location $x_\beta = 0.33$ nm, given $k_BT \approx 4.08$ pN · nm) and the characteristic unfolding rate $n/t_o \approx 2 \times 10^{-4}$/s. On the other hand, a direct linear fit to the experimental data yields at least a 100-fold larger value for the characteristic unfolding rate n/t_o and a slightly larger value for thermal force f_β. Compliance of the titin chain affects the unfolding force at all extension speeds, but most prominently at low speed. Of particular note are the LOT experiments of Kellermayer et al. (1997), which lie on the discontinuous jump predicted for this type of soft polymer linkage. Moreover, given the correlation in Fig. 8, we can estimate the rate of force increase that should accompany steady hysteretic elongation of titin. By using the thermal force f_β (12.5 pN) and an order-of-magnitude estimate for n (10^2), the rate of force increase is calculated to be $(f_\beta/n)v_t/L_{Ig} \approx 0.27$ pN/s at a speed of ~65 nm/s, which is very close to the value of ~0.3 pN/s observed in the LOT tests of Kellermayer et al. (1997).

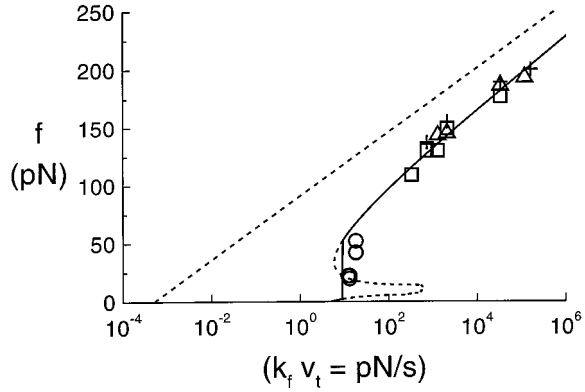

FIGURE 8 Correlation of the initial unfolding force versus log(apparent loading rate) predicted for n identical sites along a WLC polymer with a compliance parameter of $c_p \approx 10^3$ (cf. Fig. 5 *b*) to the experimental data (*discrete symbols*) from AFM and LOT tests described in Fig. 2. Matching the experimental force and apparent loading rate scales yields a thermal force $f_\beta = 12.5$ pN (equivalent to a sharp activation barrier located 0.33 nm along the force-driven pathway) and the characteristic unfolding rate $n/t_o \approx 2 \times 10^{-4}$/s. Ig domains are driven from equilibrium and resist unfolding once actual loading rates exceed the thermal activation threshold of $f_\beta n/t_o = 2.5 \times 10^{-3}$ pN/s. Determined by the parameters for f_β and n/t_o, the dashed straight line is the spectrum of unfolding force versus log(loading rate) expected if the n Ig domains were linked rigidly.

SUMMARY

We have shown that compliant linkages to bonds can significantly modify values of bond strength measured at low separation speeds and distort the entire dynamic strength image of the energy landscape of a bond. Compared to stiff linkages, a weak bond connecting polymers survives longer but is likely to fail at lower force under the same separation speed. (This conclusion was also arrived at recently by Oberhauser et al. (1998), although the range of their experiments and Monte Carlo simulations was not sufficient to capture the abrupt transition in strength at slow pulling speeds demonstrated here.) Even at higher separation speeds with polymer linkages, the linear regime of strength versus log(separation speed) deviates from the true slope, which significantly alters the characteristic kinetic rate implied by extrapolation to zero strength. Using results from AFM and LOT tests of titin extension, we have demonstrated that the unifying dynamic scale is the apparent loading rate defined by transducer stiffness × separation speed and that the effect of linkage compliance can be parameterized by a characteristic ratio of transducer:polymer stiffness.

APPENDIX

To treat polymer extension as quasielastic, pulling speed has to be sufficiently slow that polymer configurations are adequately randomized by

thermal excitations. As such, the rate of polymer extension $v_t/x_p(t)$ has to be less than the rate of thermal randomization, which we will define by $1/t_\beta$. In the classic Rouse approximation of a freely jointed chain (Doi and Edwards, 1986), the characteristic time t_β is determined by diffusion of segments over the scale of the chain length L_p, which yields $t_\beta \approx \eta L_p^2 b/k_B T$, given η as viscosity and b as segment length. Hence, the FJC polymer should behave quasielastically when $k_B T/\eta b L_p^2 \gg v_t/x_p$. Taking the initial length as the root mean square end-to-end length of an ideal chain, $x_p/L_p > (b/L_p)^{1/2}$, the criterion for quasielastic response is $(\eta v_t/k_B T)L_p^{3/2} b^{1/2} \ll 1$.

For a wormlike chain, the dynamics are governed by relaxation of thermally excited bending modes. At thermal equilibrium, the spectrum of mean square amplitudes under extension is approximated by (Fixman and Kovac, 1973; Marko and Siggia, 1995)

$$\langle u_q^2 \rangle \approx k_B T \cdot L_p^3/[\kappa_c q^4 + (f \cdot L_p^2) q^2]$$

where the bending rigidity κ_c of the chain sets the persistence length b, i.e., $\kappa_c \approx k_B T \cdot b$; the external force applied to the chain is f; and $q = 2\pi L_p/\lambda$ is the dimensionless wave number for the wavelength mode λ. To estimate the characteristic time needed for thermal randomization, we consider the relaxation time of the longest wavelength dominated by bending under force, i.e., $\lambda_b \approx 2\pi(k_B T \cdot b/f)^{1/2}$. This mode is expected to relax on a time scale of $t_\beta \approx \eta(\lambda_b/2\pi)^4/k_B T \cdot b = \eta(k_B T \cdot b/f^2)$; shorter wavelengths relax much faster. If the WLC polymer is to behave quasielastically, then $x_p/v_t \gg t_\beta$ or $1 \gg (\eta v_t/k_B T)L_p^2(b/x_p)^3$, because force scales as $f \approx (k_B T/bL_p)x_p$. Again approximating the initial length by the root mean square end-to-end length of an ideal chain, $x_p/L_p > (b/L_p)^{1/2}$, the criterion for quasielastic response is $(\eta v_t/k_B T)L_p^{1/2} b^{3/2} \ll 1$. For the fastest extension ($v_t \approx 10^3$ nm/s) of titin chains in AFM tests, the ratio $(\eta v_t/k_B T)L_p^{1/2} b^{3/2}$ is $\sim 10^{-6}$ to 10^{-5}, given the range of dimensions $L_p \approx 200$–5000 nm and $b \approx 0.4$–1 nm attributed to titin (Reif et al., 1997; Kellermayer et al., 1997) and the value of $\eta/k_B T = 2.45 \times 10^{-10}$ s/nm^3 for water.

This work was supported by U.S. National Institutes of Health grants HL31579 and HL 54700.

REFERENCES

Bell, G. I. 1978. Models for the specific adhesion of cells to cells. *Science.* 200:618–627.

Doi, M., and S. F. Edwards. 1986. The Theory of Polymer Dynamics. Clarendon Press, Oxford. 391.

Erickson, H. P. 1997. Stretching single protein molecules: titin is a weird spring. *Science.* 276:1090–1092.

Evans, E., and K. Ritchie. 1997. Dynamic strength of molecular adhesion bonds. *Biophys. J.* 72:1541–1555.

Evans, E., K. Ritchie, and R. Merkel. 1995. Sensitive force technique to probe molecular adhesion and structural linkages at biological interfaces. *Biophys. J.* 68:2580–2587.

Fixman, M., and J. Kovac. 1973. Polymer conformational statistics. III. Modified Gaussian models with stiff chains. *J. Chem. Phys.* 58: 1564–1568.

Hanggi, P., P. Talkner, and M. Borkovec. 1990. Reaction-rate theory: fifty years after Kramers. *Rev. Mod. Phys.* 62:251–342.

Kellermayer, M. S. Z., S. B. Smith, H. L. Granzier, and C. Bustamante. 1997. Folding-unfolding transitions in single titin molecules characterized with lazer tweezers. *Science.* 276:1112–1116.

Kramers, H. A. 1940. Brownian motion in a field of force and the diffusion model of chemical reactions. *Physica (Utrecht).* 7:284–304.

Marko, J. F., and E. D. Siggia. 1995. Stretching DNA. *Macromolecules.* 28:8759–8770.

Merkel, R., P. Nassoy, A. Leung, K. Ritchie, and E. Evans. 1999. Energy landscapes of receptor ligand bonds explored with dynamic force spectroscopy. *Nature.* 397:50–53.

Oberhauser, A. F., P. E. Marszalek, H. P. Erickson, and J. M. Fernandez. 1998. The molecular elasticity of the extracellular matrix protein tenascin. *Nature.* 393:181–185.

Reif, M., M. Gautel, F. Oesterhelt, J. M. Fernandez, and H. E. Gaub. 1997. Reversible unfolding of individual titin Ig-domains by AFM. *Science.* 276:1109–1112.

Seifert, U., W. Wintz, and P. Nelson. 1996. Straightening of thermal fluctuations in semi-flexible polymers by applied tension. *Phys. Rev. Lett.* 77:5389–5392.

Tskhovrebova, L., J. Trinick, J. A. Sleep, and R. M. Simmons. 1997. Elasticity and unfolding of single molecules of the giant muscle protein titin. *Nature.* 387:308–312.